ORIGINAL PAPER

Synthesis and characterization of polypyrrole–magnetite–vitamin B12 hybrid composite electrodes

Csaba Janaky · Balazs Endrodi · Angela Hajdu · Csaba Visy

Abstract In this study vitamin B12 covered magnetite nanoparticles have been incorporated into a conducting polypyrrole. This polymer was electrochemically synthesized in the presence of the B12-coated magnetite. The adsorption of B12 was demonstrated by the decrease in absorbance of the vitamin in the supernatant liquid after B12 has been in contact with magnetite sol overnight. The composition of the layers was studied by the electrochemical quartz crystal microbalance technique during the polymerization. The slope of the mass change–charge curves indicate the incorporation of 27 m/m% magnetite and 15 m/m% B12. The redox transformation of the film in monomer- and nanoparticle-free solutions was also investigated by this method and the difference in the virtual molar masses of the moving species was evidenced. The morphology and the composition of the layers were characterized by scanning electron microscopy combined with energy dispersive X-ray microanalysis measurements, which latter proved the successful incorporation of the magnetic and bio-active components. The electrochemical behavior of the films unambiguously showed the complex redox activity of the composites and the current surplus were quantified by the redox capacity of the layers. These data show the doubling of the redox capacity in case of the hybrid material compared to the neat polymer. The successful enrichment of B12 can be exploited in the recently evidenced redox mediation process performed by a PPy/B12 film.

C. Janaky · B. Endrodi · C. Visy (✉)
Institute of Physical Chemistry, University of Szeged,
Rerrich square 1,
Szeged 6720, Hungary
e-mail: visy@chem.u-szeged.hu

A. Hajdu
Department of Colloid Chemistry, University of Szeged,
Aradi square 1,
Szeged 6720, Hungary

Introduction

Organic–inorganic nanocomposites with an ordered structure provide new functional hybrids of organic and inorganic materials. Incorporation of nanosized particles in organic polymeric materials has been extensively studied because they combine the advantages of the inorganic materials and the organic polymers. Moreover, due to synergetic effects, also new properties can show up, which can be scarcely obtained from the individual components. Conducting polymers have been already combined with metals, metal-oxides, and other compounds [1, 2].

Combination of different conducting polymers with magnetic iron-oxides is more and more intensively studied, because materials possessing both high magnetic susceptibility and high conductivity can be used in different applications, such as nonlinear optics, electrical, and magnetic shielding, magnetic electrocatalysis, and as microwave absorbers [3]. Magnetite (Fe_3O_4) nanolayers are prominent candidates for electrocatalytic applications, due to the redox switching between Fe^{3+}/Fe^{2+}. This behavior can be used in different catalytic processes, such as O_2 or H_2O_2 reduction [4, 5]. Polypyrrole–iron-oxide composites are used also as electrochemical supercapacitators [6–8]. In addition, due to the large surface area, magnetic nanoparticles tend to adsorb a wide sort of molecules to minimize their surface free-

Table 1 Concentrations and polymerization charges applied during the synthesis of different samples

	Magnetite (g dm^{-3})	B12 (M)	Q (mC cm^{-2})
Sample 1	0	0	90
Sample 2	10	0	90
Sample 3	10	0.01	90
Sample 4	0	0	300
Sample 5	10	0	300
Sample 6	2.5	0.01	150
Sample 7	5	0.01	150
Sample 8	10	0.01	60/150/300

The constant concentration of pyrrole and PTO was 0.1 and 0.05 M, respectively

energy. The adsorption of different biomolecules—including hemoglobin, DNA, and different enzymes—on magnetite surface has been reviewed recently [9].

For electrocatalytic and other electrochemical applications the electropolymerization is the best way to prepare these composites films, directly on the electrode surface. In the literature, a few papers report on the electrochemical preparation of conjugated polymer–magnetic nanoparticle composites in aqueous [10–12] and non-aqueous solution [13]. A successful immobilization is always related to an interaction between the nanoparticles and the monomer/doping ion. Recently, Deslouis and his co-workers reported on an easy synthesis route of polypyrrole–magnetite nanocomposite layer [14] by using potassium-tetraoxalate as conducting electrolyte, where the hydrogen-oxalate monovalent anions acted as dopants.

In different bio-electrochemical processes, mediators are used frequently [15], which can promote the electron transfer between the electrode and the bioactive species, e.g. an enzyme. Different biomolecules have been immobilized into conducting polymers [16, 17] for various applications, such as sensing or mediation. Vitamin B12 is one of these mediators, exhibiting a rather complicated redox activity connected to its cobalt center. This activity has been applied in several catalytic and sensing procedures [18–20]. In the last few years, some successful attempts have been realized for the immobilization of vitamin B12 into conducting polymer films. This is an important issue, due to the fact that an electroactive enzyme can be wired this way to the electrode. The accumulation was achieved through different methods: in one case with special pyrrole derivatives, where a chemical bond was formed between the monomer and B12 [21], while in another example the interaction between the doping anions (PIPES) and B12 lead to the composite formation [22].

In this paper, we report on the electrochemical synthesis of polypyrrole–magnetite–B12 bio-nanocomposite layers. To

achieve this aim, we took the advantageous properties of magnetite: while vitamin B12 adsorbs on its surface (as our preliminary results showed), these nanoparticles can be easily incorporated into the polymeric film. With this method, we can fill the conducting layer both with magnetically and biologically active compounds. It is important to emphasize that all the components show redox activity in the same potential region, this way—due to synergetic effects—an advanced electrode activity can be expected.

## Experimental part

Synthesis of magnetite nanoparticles

Magnetite (Fe_3O_4) nanoparticles were synthesized by alkaline hydrolysis of iron(II) and iron(III) salts ($FeCl_2 \times 4H_2O$ and $FeCl_3 \times 6H_2O$, Reanal, Hungary) [23, 24]. The synthesis resulted magnetite nanoparticles with an average size around 10 nm. The characterization of the as prepared particles was reported elsewhere [25].

Adsorption of B12 molecules on magnetite

Adsorption experiment have been carried out by preparing six samples with a constant magnetite amount 10 g dm^{-3} and varying the concentration of vitamin B12 between (0.02–0.002 M). These samples were left to interact for 24 h, than they were centrifuged to have the supernatant phase. After having registered the calibration curve (which showed a linear, Beer–Lambert relation), UV-visible spectra of the previously treated and diluted samples were recorded. The adsorption isotherm was calculated from the decrease in absorbance of the samples at 362 nm.
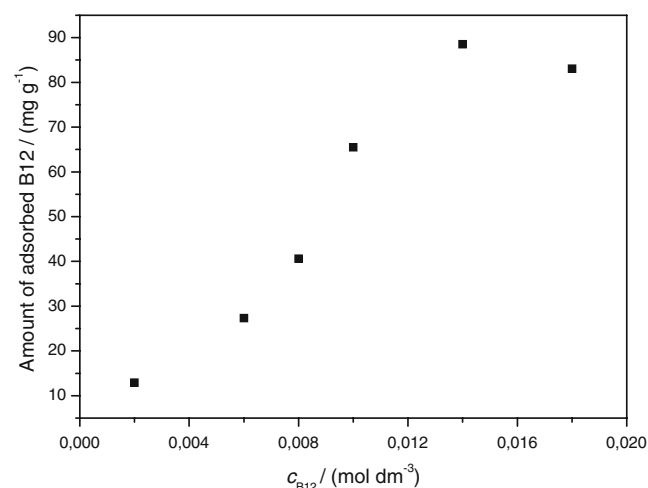
Fig. 1 The equilibrium adsorption isotherm for vitamin B12 (in the concentration range up to 0.02 M) on magnetite nanoparticles in aqueous sol, at a concentration of 10 g dm^{-3}
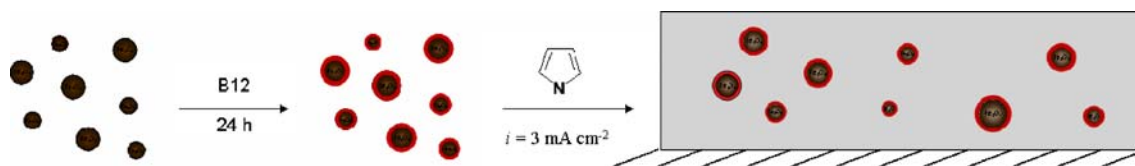
Scheme 1 Illustration of the adsorption of B12 on magnetite surface and the synthesis of hybrid composite layer through electrochemical polymerization

Preparation of thin bio-nanocomposite layers

Pyrrole (Py) monomer, potassium-tetraoxalate (PTO) and Vitamin B12 were purchased from Sigma-Aldrich. All chemicals were from analytical grade. Pyrrole was freshly distilled before use.

Polypyrrole (PPy), polypyrrole–magnetite, and polypyrrole–magnetite–B12 composite thin films were deposited galvanostatically at a 3 mA cm^{-2} current density onto platinum electrode (A=2.00 cm^2) and platinum covered quartz crystal electrode (f_0=10 MHz, A=0.1964 cm^2). All polymerization solutions contained 0.1 M of the monomer pyrrole, 0.05 M PTO and 0.01 M B12 in water (pH=1.5). The amount of magnetite particles varied between 2.5 to 10 g dm^{-3} in three steps (2.5, 5, and 10 g dm^{-3}). For further voltammetric studies, the solution was changed after the polymerization to a monomer-, magnetite-, and B12-free solution of PTO in water. In case of the electrochemical quartz crystal microbalance (EQCM) measurements, charge density was restricted to 90 mC cm^{-2}, in order to avoid viscoelastic effects [26], in other cases it was 150 and 300 mC cm^{-2}. For the transmission electron microscopy (TEM) analysis, thinner layers were prepared under identical conditions, with a 60 mC cm^{-2} charge density. The circumstances of the different polymerizations are summarized in Table 1 and the schematic view of the synthetic procedure is presented in Scheme 1.

Characterization techniques

The electrochemical measurements were performed on a PGSTAT 10 (Autolab) instrument, in a classical three electrode electrochemical cell. The working electrode was platinum electrode and platinum-covered quartz crystal electrode (f_0=10 MHz). Ag/AgCl reference electrode was used, having a potential 0.200 V vs. SHE. All the potential values in the paper are given with respect of the silver/silver chloride electrode. The EQCM measurements were performed using a quartz crystal resonator and analyser EQCM type 5510 (Poland). The EQCM system was calibrated by electrochemical silver deposition using the standard procedure and the value of −0.86 ng Hz^{-1} calibration constant was obtained. Cyclic voltammograms of the thin films were registered in 0.05 M PTO monomer-free solutions at different sweep rates between 10 and 100 mV s^{-1}.

Hitachi S-4700 scanning electron microscopy (SEM) coupled with energy-dispersive X-ray (EDX) spectroscopy (Röntec QX2) was used to investigate the morphology of the samples, resulting also in information of their elementary composition.

Transmission electron microscopy was performed using a Philips CM 10, operating at an acceleration voltage of 100 kV.

UV-Vis spectroscopic measurements were carried out in solutions using an Agilent 8453 UV-Visible Spectrophotometer.

Results and discussion

Adsorption of B12 on magnetite nanoparticles

The obtained adsorption isotherm is presented in Fig. 1. The isotherm has a typical pattern, where the saturation is achieved over the concentration of 0.01 M. It is assumed that the detected adsorption is due to physisorption between the biomolecules and the nanoparticles having large surface area. The physisorption might be the consequence of
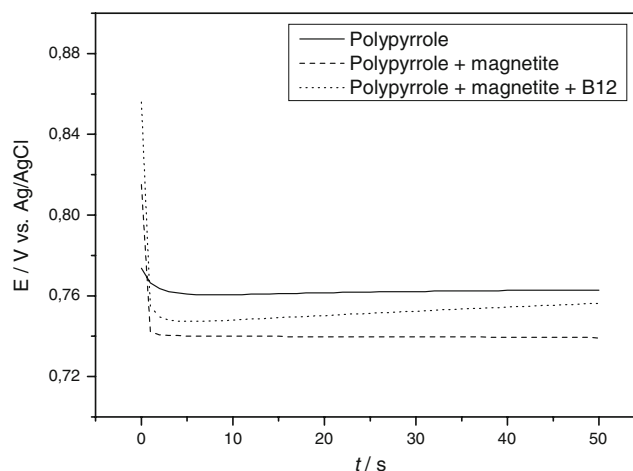
Fig. 2 Chronopotentiometric E–t curves obtained during the galvanostatic polymerization (i=3 mA cm^{-2}) of pyrrole in case of sample 4, 5, and 8. The concentration of pyrrole and PTO was always 0.1 and 0.05 M, respectively (pH=1.5). In case of sample 5 magnetite was present at a concentration of 10 g dm^{-3}, while sample 8 contained also 0.01 M B12
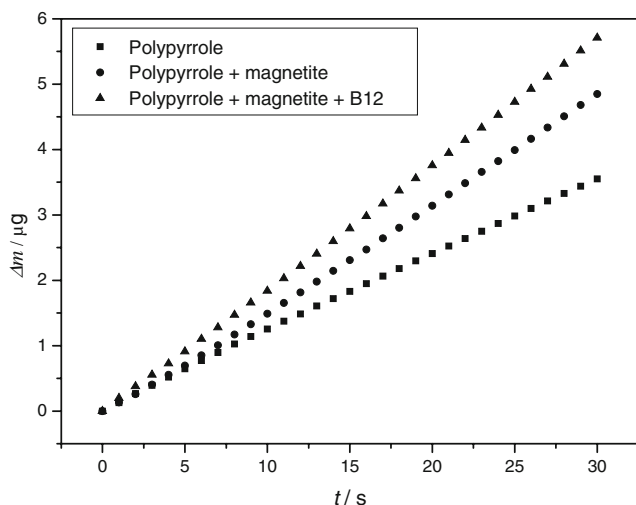
Fig. 3 Comparison of the mass changes obtained under identical (polymerization) conditions, as in Fig. 2

dipole–dipole interactions existing between the functional groups of B12 and the polar particle surface. Moreover hydrogen-bond formation can also take place, as it has been reported elsewhere for other B12-containing systems [27]. Based on the results, we decided to synthesize our samples at a concentration 0.01 M for B12, because the magnetite particles are almost totally covered with the bio-active component.

Chemical composition

The chemical composition of the neat polymer and the different composite films were compared with materials synthesized under totally identical electrochemical conditions. In Fig. 2, chronopotentiometric curves registered during the galvanostatic polymerization are presented. Their similarity, the reproduction within a 20 mV range

without a rigorous trend give the evidence that the polymerization process is not disturbed by iron oxide sol in case of the composite formation.

EQCM measurements were performed to get information about the composition of the electrochemically deposited films. The mass increase of the layers vs. the transferred charge is linear for all samples as shown in Fig. 3. In this figure, three cases are compared: the neat polypyrrole (sample 1), the film polymerized in the presence of magnetite (sample 2), and the film prepared with magnetite, covered with adsorbed B12 (sample 3). The good linearity of the curves can be related to the monotonous growth of the films and to the assumingly uniform particle incorporation. At the same time, the difference between the cases is striking; the slope of the curves is gradually increasing, proving that magnetite and magnetite + B12 are embedded during the polymerization. From the slope values, the relative amount of the built-in materials can be calculated, for which 26.7 m/m% magnetite and 15.0 m/m% B12 were obtained. A similar incorporation ratio for magnetite was obtained also previously [13]. The 15 m/m% value, resulted for B12, is much higher than it could have been expected from the adsorbed amounts, determined previously. We assume that the incorporation of B12-covered magnetite nanoparticles promotes also the immobilization of free vitamin B12 molecules into the polymeric layer.

Further evidence for the successful immobilization of the different additives could be obtained from EDX data (Fig. 4). Although the signal of the platinum support is dominant, the characteristic peaks for C, N, O, and Fe are clearly visible. If we enlarge the relevant region, we could detect a peak at 6.9 keV which at least partially should originate from Co. Anyway, since B12 is proved to be adsorbed on Fe_3O_4 nanoparticles, the presence of Fe peak indirectly serves as a proof for the immobilization of B12 as well.

Fig. 4 EDX spectra of a nanocomposite layer deposited on platinum electrode with a charge density of 300 mC cm^{-2}. The *insert* shows the relevant area, with the peaks related to Fe and Co
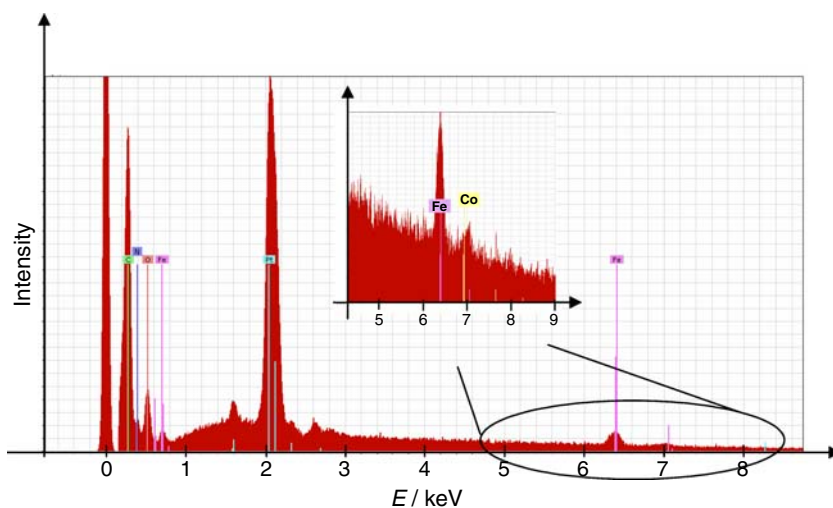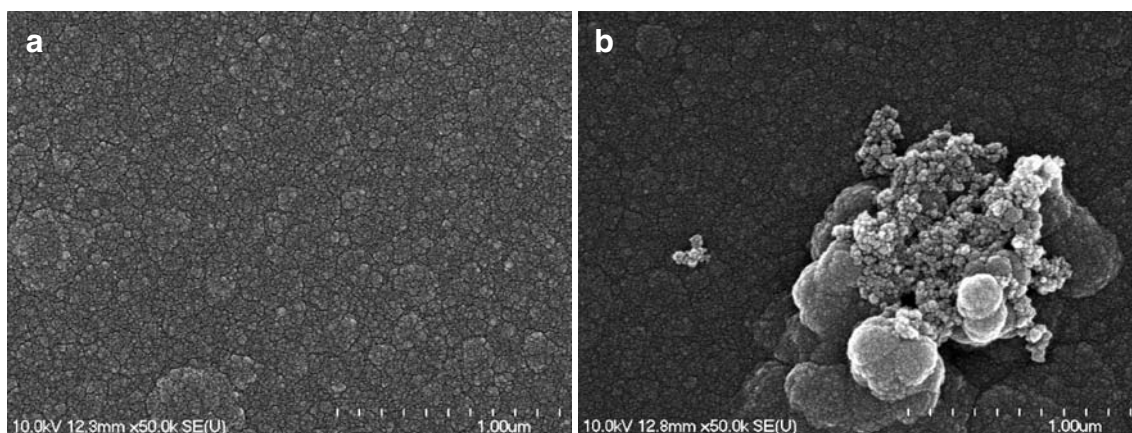
Fig. 5 **a** SEM image of neat polypyrrole at ×50,000 magnification. **b** SEM image of the polypyrrole–magnetite–B12 nanocomposite at ×50,000 magnification

Supramolecular structure and surface morphology

Scanning electron microscopy was used to study the morphology of the prepared films. The images recorded at ×50,000 magnification are presented in Fig. 5a for the neat polymer and in Fig. 5b for the B12-containing layer. The morphology of both samples is similar, the well-known randomly varying surface, consisting of globular, cauliflower-like units is visible. On the other hand, in contrast to the rough morphology generally obtained for polypyrrole, our (oxalate-doped) samples seems to be rather smooth, even in the sub-micrometer dimension. If we compare the two pictures, one important difference can be observed: in case of the composite material aggregated magnetite particles are visible on the polymer surface, attached to the globular shape polymeric particles outgrown from the layer. This image proves that magnetite particles are not only incorporated into the polypyrrole film during the polymerization, but they are adsorbed on the polymer film as well.
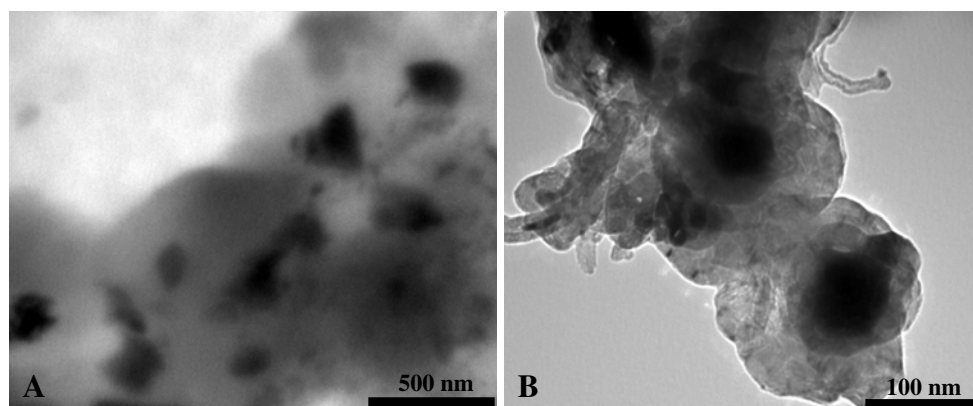
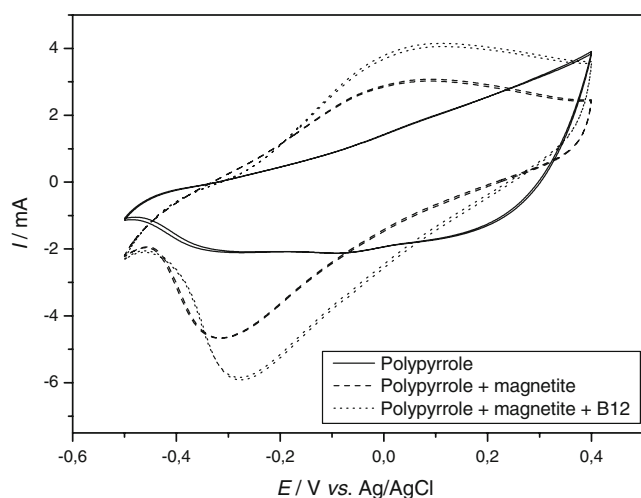When we studied a very thin layer of the composite by transmission electron microscopy, we could observe the randomly distributed dark spots originating from the incorporated particles. Both Fig. 6a, b proves the encapsulation of magnetite into the polymeric layer. Although at certain regions the primary sized particles can be revealed, their aggregation can be also detected, which is not surprising, because no surfactant was used during the synthesis, to avoid the competing adsorption with B12.

Electrochemical studies

Electrochemical properties of the layers have been investigated by cyclic voltammetry, performed at different sweep rates between 10–100 mV s^{-1}. In Fig. 7, voltammograms of the neat polymer (sample 4) and the composite samples (sample 5 and 8) are compared. The curve obtained with polypyrrole itself reflects relatively weak redox behavior, assumingly due to the poor quality of the film. This behavior has been already reported for this system, and was explained as a result of the doping by oxalate ions [13]. In the two other cases, we have similarly good electrode activities, but with significantly higher currents in the case of the B12-containing bio-nanocomposite layer. Since this

Fig. 6 **a** TEM image of thin hybrid composite layer (sample 8) at ×19,000 magnification. **b** TEM image of thin hybrid composite layer (sample 8), at ×130,000 magnification

Fig. 7 Comparison of cyclic voltammograms at 50 mV s^{-1} sweep rate for neat polypyrrole, polypyrrole–magnetite and polypyrrole–magnetite–B12 in 0.05 M PTO solution at pH=1.5

even being built in a polymer matrix in the adsorption sphere of a magnetic component.

In order to see how the magnetite content of the polymerization sol effects the incorporation of B12, we prepared composites at different Fe_3O_4 concentrations (sample 6–8). In all cases a considerable extra current was registered compared to the B12-free reference cases (sample 4–5). But this extra current was always the same since, surprisingly, we found that the voltammetric curves are practically the same. It means that the surplus originating from B12 is independent from Fe_3O_4 content. It may be assumed that already 2.5 g dm^{-3} magnetite amount is enough to saturate the polymer layer. Furthermore, 0.01 M concentration of B12 is more than enough to reach the total coverage on magnetite nanoparticles even at the largest (10 g dm^{-3}) concentration.

EQCM measurements during the redox transformation of the layers are expected to give information on the processes on the molecular level [34]. With this method, the virtual molar mass of the moving species can be determined. A typical set of I–E, Δm–E curves during the voltammetric study at 50 mV s^{-1} for the polymer and the bio-nanocomposite is presented in Figs. 8 and 9. One can see that the oxidation is related to a monotonous mass increase, while during the reduction a mass decrease can be observed. Thus, the doping process is accompanied dominantly by the movement of anions in both cases. To quantify this process, we derived the Δm–q curves from the data presented in Figs. 8 and 9. The slope of these curves directly supplies the above mentioned virtual molar mass value. In Fig. 10, three subsequent cycles are presented for sample 3. Apart from the reduction end, the curve is linear for both the anodic and cathodic sections, and a slope of ~94 gmol^{-1} was obtained. For comparison, similar calculation led to ~58 gmol^{-1} and ~95 gmol^{-1} for sample 1–2. (All these values were calculated as an average of data obtained with different layers and scans.) If we compare these values to the molar mass of oxalate anion (89 g mol^{-1}), we may assume that oxalate anion is the moving species in the cases of magnetite containing layers. As for the 58 gmol^{-1} value, obtained in the case of neat

current surplus is permanently sustained during continuous cycling, it should be the consequence of the electro-activity of iron-oxide and B12 in this potential region [28–31]. Such an extra current obtained after the incorporation of B12 could be used to mediate cathodic reduction [32]. To quantify the differences in the basic electrochemical behavior of the films, the redox capacities of each layer, obtained at different sweep rates, are summarized in Table 2, where the transferred charges during complete redox cycles are compared. As the table shows, the presence of magnetite results in a 30–70% increase, changing inversely with the scan rate. This fact suggests the capacitive pattern [33] of this charge component, typical for iron oxides [28, 29]. As for the incorporated B12, it causes an additional 30–40% increment compared to the neat polymer. This increment is independent from the sweep rate, which may indicate its faradic origin and can be related to the complicated redox activity of B12. The vitamin can be reduced in this potential region, its actual value strongly depends on the chemical surroundings of the molecule, whether it is in solution, in self-assembled monolayer, or

Table 2 Comparison of the redox capacity of sample 4, 5, and 8 during the redox cycles at different sweep rates

|	10mV s^{-1}		25mV s^{-1}		50mV s^{-1}	
	Q_{total} (mC)	Relative Q(%)	Q_{total} (mC)	Relative Q (%)	Q_{total} (mC)	Relative Q (%)
Polypyrrole (sample 4)	74.1	100	62.3	100	56.1	100
Polypyrrole + Fe_3O_4 (sample 5)	126.1	170.1	94.9	152.3	70.9	126.4
Polypyrrole + Fe_3O_4 + B12 (sample 8)	146.1	197.1	121.5	195.2	92.6	165.1
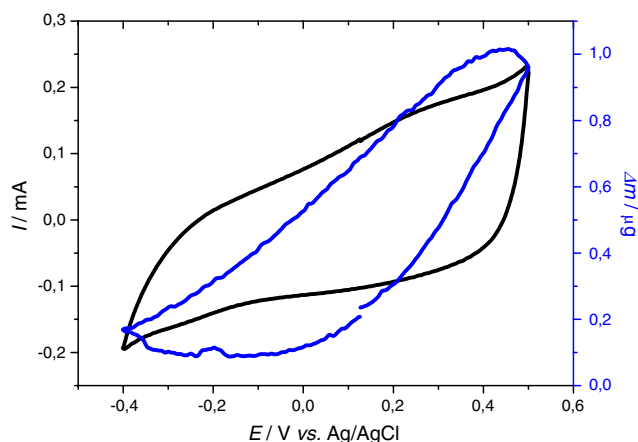
Fig. 8 Voltammetric curve and the coupled mass changes registered with the neat polypyrrole (sample 1) during the cycling at a 50 mV s⁻¹ scan rate in 0.05 M PTO solution at pH=1.5

polypyrrole, it is considerably smaller than the molar mass of the anion itself. This lack of mass could be connected to parallel cationic and/or solvent movements [35–37]. Although cationic movements may often participate in the charge compensation, but in case of polypyrrole only over pH=3–4 [37]. As the pH of our solution was always below pH=2, cationic doping should not be considered. Moreover, the linearity of the $\Delta m/q$ curves indicates also the permanent movement of a single anion, even in the more negative potential region, where cationic contribution could be expected. Although the interpretation of the phenomenon is beyond the topic of this work, the results suggest that the anion incorporation can be coupled with the removal or expulsion of water molecules from the layer. The effect may be interpreted by an obvious difference in the hydrophobicity of the neat polypyrrole and the iron-oxide-containing polymeric film.
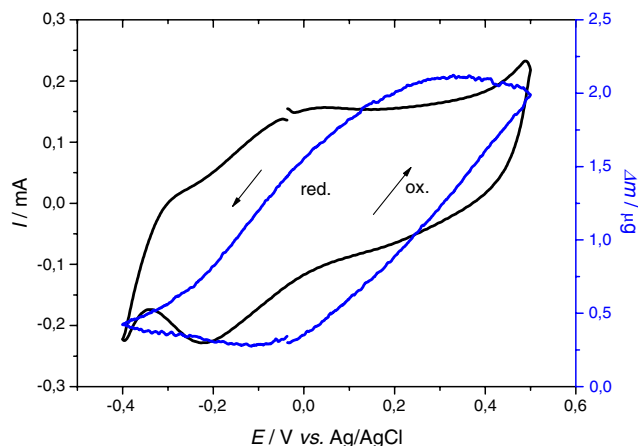
Fig. 9 Voltammetric curve and the coupled mass changes registered with the bio-nanocomposite layer (sample 3) during the cycling at a 50 mV s⁻¹ scan rate in 0.05 M PTO solution at pH=1.5
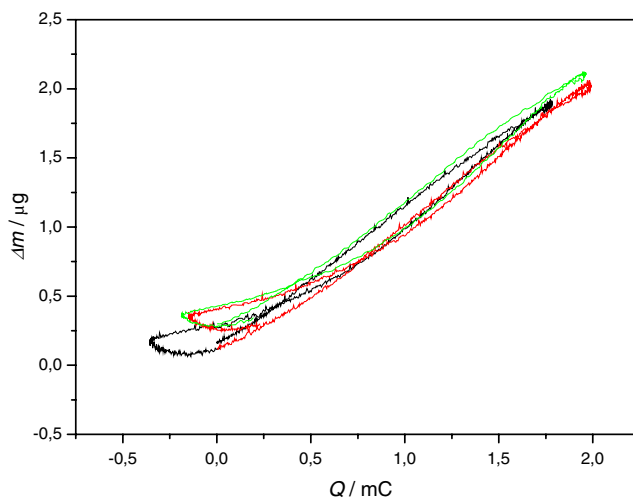
Fig. 10 Mass change vs. transferred charge curves calculated from EQCM data presented in Fig. 9 for three subsequent cycles of the hybrid composite layer

Conclusions

In this work we give a report on the successful synthesis of PPy/Fe₃O₄/B12 nanocomposite layers. EQCM data acquired during the polymerization lead to the conclusion that 27 m/m% magnetite and 15 m/m% B12 was incorporated into the layer. These values are well reproducible in different experiments, and indicate the maximally attainable composition under our circumstances. The immobilization of vitamin B12 was performed by realizing its adsorption on the magnetite nanoparticles. The adsorption takes place through a physisorption based assumingly on dipole–dipole interactions existing between the functional groups of B12 and the polar particle surface.

The prepared hybrid composite layers have significantly higher electroactivity in comparison to the neat samples. At low sweep rates, this surplus results in a two times larger value in the charge capacity in case of the hybrid layer. The observed charge surplus can be connected partially to the capacitive behavior of the incorporated magnetite, which pattern is well indicated by its dependence on the scan rate. On the other hand, the extra charge originates from the redox activity of the immobilized vitamin, too.

The above described results demonstrate how B12 can be accumulated in conducting polymer films through composite formation. As the redox mediation ability of the PPy/B12 film was recently evidenced, we hope that the application of this novel hybrid may lead to enhanced performance in mediated cathodic processes.

References

1. Gomez-Romero P (2001) Adv Mater 13:163. doi:10.1002/1521-4095(200102) 13:3<163::AID-ADMA163>3.0.CO;2-U
2. Kickelbick G (2003) Prog Polym Sci 28:83. doi:10.1016/S0079-6700(02)00019-9
3. Gangopadhyay R, De A (2000) Chem Mater 12:608. doi:10.1021/cm990537f
4. Vago ER, Calvo EJ (1992) J Electroanal Chem 339:41. doi:10.1016/0022-0728(92)80444-9
5. Zhao G, Xu JJ, Chen HY (2006) Electrochem Commun 8:148. doi:10.1016/j.elecom.2005.11.001
6. Manuel J, Kim JK, Ahn JH et al (2008) J Power Sources 184:527. doi:10.1016/j.jpowsour.2008.02.079
7. Kwon CW, Poquet A, Mornet S et al (2002) Electrochem Commun 4:197. doi:10.1016/S1388-2481(02)00250-3
8. Mallouki M, Sarrazin C, Simon P et al (2007) J Solid State Electrochem 11:398. doi:10.1007/s10008-006-0161-8
9. Katz E, Willner I (2004) Angew Chem Int Ed 45:6042. doi:10.1002/anie.200400651
10. Garcia B, Lamzoudi A, Deslouis C et al (2002) J Electrochem Soc 149:B560. doi:10.1149/1.1517581
11. Bidan G, Jarjayes O, Fruchart F et al (1994) Adv Mater 6:152. doi:10.1002/adma.19940060213
12. Jarjayes O, Fries PH, Bidan G (1995) Synth Met 69:343. doi:10.1016/0379-6779(94)02477-G
13. Janaky C, Visy C, Berkesi O et al (2009) J Phys Chem C 113:1352. doi:10.1021/jp809345b
14. Pailleret A, Hien NTL, Deslouis C (2007) J Solid State Electrochem 11:1013. doi:10.1007/s10008-007-0262-z
15. Giuseppi-Elie A, Wallace GG, Matsue T (1998) In: Skotheim TA, Elsenbauer RL, Reynolds JR (Eds) Handbook of Conducting Polymers, p. 963, Marcel Dekker, New York
16. Cosnier S (1999) Biosens Bioelectron 14:443. doi:10.1016/S0956-5663(99)00024-X
17. Ahuja T, Mir IA, Kumar D et al (2007) Biomaterials 28:791. doi:10.1016/j.biomaterials.2006.09.046
18. Ramanavicius A, Ramanaviciene A, Malinauskas A (2006) Electrochim Acta 51:6025. doi:10.1016/j.electacta.2005.11.052
19. Brown KL (2005) Chem Rev 105:2075. doi:10.1021/cr030720z
20. Shimakoshi H, Nakazato A, Hayashi T et al (2001) J Electroanal Chem 507:170. doi:10.1016/S0022-0728(01)00418-1
21. Fraga R, Correia JP, Abrantes LM et al (2005) Electrochim Acta 50:1653. doi:10.1016/j.electacta.2004.10.059
22. Visy C, Csízi I, Kriván E (2007) Electrochim Acta 53:1190. doi:10.1016/j.electacta.2006.12.069
23. Illés E, Tombácz E (2003) Colloids Surf A Physicochem Eng Asp 230:99. doi:10.1016/j.colsurfa.2003.09.017
24. Illés E, Tombácz E (2006) J Colloid Interface Sci 295:115. doi:10.1016/j.jcis.2005.08.003
25. Tombácz E, Illés E, Majzik A et al (2007) Croat Chem Acta 80:503
26. Skompska M, Jackson A, Hillman AR (2000) PCCP 20:4748
27. Goo Z, Zhu G, Qiu S et al (2005) Carbon 43:2344. doi:10.1016/j.carbon.2005.04.014
28. Nagarajan N, Zhitomirsky I (2006) J Appl Electrochem 36:1399. doi:10.1007/s10800-006-9232-x
29. Wang SY, Ho KC, Kuo SL et al (2006) J Electrochem Soc 153:A75. doi:10.1149/1.2131820
30. Lexa D, Saveant JM (1983) Acc Chem Res 16:235. doi:10.1021/ar00091a001
31. Yang N, Wan Q, Wang X (2005) Electrochim Acta 50:2175. doi:10.1016/j.electacta.2004.09.026
32. Markusova K, Fedurco M (1991) Anal Chim Acta 248:109. doi:10.1016/S0003-2670(00)80875-2
33. Bard AJ, Faulkner LR (2001) Electrochemical Methods, Fundamentals and Applications, 2nd edn. Wiley, New York
34. Weidlich C, Mangold KM, Juttner K (2005) Electrochim Acta 50:1547. doi:10.1016/j.electacta.2004.10.032
35. Plieth W, Bund A, Rammelt U et al (2006) Electrochim Acta 51:2366. doi:10.1016/j.electacta.2005.03.087
36. Visy C, Janaky C, Krivan E (2005) J Solid State Electrochem 9:330. doi:10.1007/s10008-005-0661-y
37. Xie Q, Kuwabata S, Yoneyama H (1997) J Electroanal Chem 420:219. doi:10.1016/S0022-0728(96)04777-8